Table 1

M_1	δ_1^*/δ_1
0	0.13
1	0.16
2	0.24
3	0.33

proximately given by Ref. 11 for a zero pressure gradient boundary layer.

$$\delta_1^* = \frac{0.0475(1 + 0.35M_1^2)x_1}{[1 + 0.88[(\gamma - 1)/2]M_1^2]^{0.44}(Gx_1/A_1\mu_1)^{0.2}} \quad \text{(A9)}$$

References

[1] Louis, J. F., Lothrop, J., and Brogan, T. R., "Fluid dynamic studies with a magnetohydrodynamic generator," Phys. Fluids **7**, 362 (1964).

[2] Hurwitz, H., Kilb, L. W., and Sutton, G. W., "Influence of tensor conductivity on current distribution in a MHD generator," J. Appl. Phys. **32**, 205 (1961).

[3] Crown, J. C., "Analysis of magneto gas dynamic generators having segmented electrodes and anisotropic conductivity," United Aircraft Rept. R 1852-2 (February 1961).

[4] Teare, J. D., "Thermodynamic equilibrium calculations for carbon-hydrogen-oxygen-nitrogen mixtures," Avco-Everett Research Lab. Rept. AMP 104 (May 1961).

[5] Louis, J. F. and Decher, R., "MHD generator performance under non-uniform and time varying load," Avco-Everett Research Lab. Research Rept. 148 (March 1963).

[6] Kantrowitz, A. R., "One-dimensional treatment of non-steady gas dynamics," *Fundamentals of Gas Dynamics*, edited by H. W. Emmons (Princeton University Press, Princeton, N. J., 1958).

[7] Mager, A., "Prediction of shock-induced turbulent boundary-layer separation," J. Aeronaut. Sci. **22**, 201 (1955).

[8] Schuh, H., "On determining turbulent boundary-layer separation in incompressible and compressible flow," J. Aeronaut. Sci. **22**, 343 (1955).

[9] Crocco, L., "One-dimensional treatment of steady gas dynamics," *Fundamentals of Gas Dynamics*, edited by H. W. Emmons (Princeton University Press, Princeton, N.J., 1958).

[10] Gadd, G. E., "Interactions between wholly laminar or wholly turbulent boundary layers and shock waves strong enough to cause separation," J. Aeronaut. Sci. **20**, 729 (1953).

[11] Monaghan, R. J., "Comparison between experimental measurement and suggested formula for the variation of turbulent skin friction in compressible flow," Great Britain Aeronautical Research Council TR C. P. 45 (1950).

[12] Arens, M. and Spiegler, E., "Shock-induced boundary layer separation in overexpanded conical exhaust nozzles," AIAA J. **1**, 578–581 (1963).

AUGUST 1965 AIAA JOURNAL VOL. 3, NO. 8

Generation and Characteristics of Plasma Wind-Tunnel Streams

DAVID F. HALL,* ROBERT F. KEMP,* AND J. M. SELLEN JR.*

TRW Space Technology Laboratories, Redondo Beach, Calif.

The plasma wind tunnel permits the laboratory study of the interaction of a moving material body with a dilute plasma, such as the ionosphere, and the laboratory calibration of spacecraft plasma diagnostic instrumentation. Plasma streams, with uniform density cross sections ~30 cm diam of H_2, He, N_2, O_2, Ne, A, CO_2, and Cs, and some mixtures thereof, have been produced at 1.6 m from an 11-cm electron bombardment and a 2.5-cm contact ion source. Except for H_2 and He, velocities and densities appropriate for simulation of a satellite in circular orbit below the heliosphere ($\leq$8 km/sec, $\leq 10^6$ ions/cm^3) are included in the range of operation of these sources. The ion velocity spread in the longitudinal direction, encountered by a satellite, caused by the ion thermal motion has been simulated through the variation of plasma source accelerating potential. Simulation of transverse velocity components caused by thermal motion has been achieved through the use of electrostatic scattering fields imposed on the stream.

Nomenclature

v_+ = ion velocity, km/sec
j_+ = ion current density, amp/cm^2
V = potential, v
$\tilde{V}$ = maximum value of perturbation potential, v
q = electric charge, coul
ΔW = width of energy distribution, ev
N = total number of particles in system
n = plasma density, ions/cm^3
k = Boltzmann's constant, 1.38×10^{-23} joules/°K
T = Kelvin temperature
M = mass, kg
r = radius, radial distance, cm
Λ = klystron bunching length, cm
L = axial length of the divergence analyzer, cm
l = source to object distance, cm
θ = maximum beam divergence angle of uniform portion

Subscripts

$+$ = ion
d = deflection
e = electron
s = spacecraft
p = plasma
pr = probe
0 = average beam value
1 = perturbation value
is = ion source
th = average thermal

Received November 9, 1964; revision received April 23, 1965. This work was supported by NASA Lewis Research Center under Contract No. NAS3-4114.

* Member of the Technical Staff. Member AIAA.

I. Introduction

A PREVIOUS paper[1] has introduced the concept of simulating spacecraft travel through ionized media by directing a low-density streaming plasma toward a stationary vehicle or model thereof. This paper will detail later techniques and refinements that enable a rather complete simulation of spacecraft travel through the ionosphere and the calibration of instruments on board for the diagnosis of the space plasma.

Section II of this paper briefly reviews the constituents of the ionosphere and typical satellite orbital velocities to indicate the required characteristics of the plasma beams that simulate satellite travel through the ionosphere. Section III describes the test facility and the diagnostic instruments and techniques used in assuring that the synthesized beams have the desired properties. Section IV discusses the ion sources and the beams that have been produced to date. Some refinements of simulation are presented in Sec. V.

II. Ionosphere and Orbital Velocities

Probably the most characteristic feature of the ionosphere is its variability. It is possible, however, to indicate typical magnitudes of mass number, ion density, and ion temperature which occur[2-5] and these, plus typical orbital velocities, will indicate the properties required of a plasma beam, that is, to simulate vehicle motion through the ionosphere.

For convenience, data obtained from Refs. 2 and 4 are reproduced in Table 1. Values of ion concentration n listed represent the approximate maxima that occur for geomagnetic latitudes near 35°. (In simulation, it is always easier to produce lower values of n.) Temperatures used to calculate average ion thermal velocity $v_{+,\mathrm{th}}$ are those of neutrals in the region. Values of v_s, the spacecraft velocity, are those for circular orbits. Higher velocities can be attained in elliptical orbits and by space probes, and lower velocities occur at apogee of probe shots that return to the earth. Values of $v_{e,\mathrm{th}}$, the average electron thermal velocity, exceed 100 km/sec and therefore will appear quite random to all orbiting spacecraft.

In general, then, simulation calls for ions of mass numbers between 14 and 32, ion densities not exceeding 3×10^6 ions/cm^3, and directed velocities between 7 and 8 km/sec. Electron velocities should be random and at least an order of magnitude greater. Simulation of the ion velocity distribution encountered in the upper heliosphere and the protonosphere will not be appropriate with the plasma wind tunnel because at that elevation, $v_{+,\mathrm{th}} \simeq v_s$, i.e., the ion motion with respect to the vehicle is not well ordered.

III. Measurement of Beam Characteristics

Some of the elements of a typical plasma wind tunnel are depicted in the sketch (Fig. 1). The facility used for these studies is a 4- × 8-ft cylindrical vacuum chamber, pumped by an oil diffusion pump to a background pressure of $\sim 2 \times 10^{-6}$ torr. This corresponds to a neutral density of 6×10^{10} particles/cm^3 and a mean free path of the order of 10^3 m. One of two plasma sources is fitted to a port in one end of the tank, and a model vehicle or other test object is located near the other end. In addition, various diagnostic devices for determining the measurable characteristics of the plasma beams are arranged in the vicinity of the test object. These beams are well neutralized, and their plasma potentials V_p are typically 5 to 20 v positive with respect to ground.[6-8]

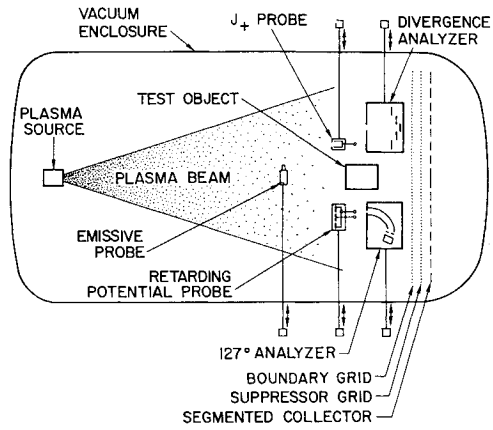

Fig. 1 Schematic diagram of the plasma wind tunnel. Diagnostic instruments and object under test may be moved from outside the vacuum enclosure.

A. Beam Current, Current Density

Total beam current at the farthest downstream location may be determined from the sum of ion currents arriving at the various elements of the collector. Segmentation allows for rough measurements of radial distribution of beam current. The accuracy of the measurement is improved by placing two grids in front of the collector. The boundary grid, maintained at the potential of the vacuum enclosure (ground), electrically shields the suppressor grid that is sufficiently negative to reflect both plasma electrons and secondaries. When beam current measurements are not being made, the collector and its grids are connected only to each other, so that they assume the "floating potential" that corresponds to collection of equal ion and electron currents from the beam. Thus, they introduce a plane unipotential surface into the beam but otherwise offer a minimum electrical interference.

Detailed mapping of beam current density is done with "Faraday-cup" probes (abbreviated j_+ probes), ranging in size from $\frac{1}{16}$ in. to several inches in diameter, which can be moved about within the beam. The small probes consist of two concentric cylinders, an outer one with a gridded entrance aperture biased to reject electrons, and an inner collection cup.[7] Folded along the vacuum tank wall is a boom (not shown) on which are mounted four similar but large and rectangular j_+ probes. This boom may be swung into the beam so that the end probe is on the tank axis. These probes have equal areas and are used to ascertain quickly the uniformity of number density n through the relation $n = j_+/qv_+$.

B. Plasma Potential

It is important to be able to determine V_p, the space potential within the plasma, because ion velocity is related

Table 1 Typical values of ionosphere variables important to simulation

Alt, km	Designation	Constituents	$n_{\max}$, ions/cm^3	$v_{+,\mathrm{th}}$, km/sec	v_s, km/sec
60–85	D	NO^+(?)	1×10^3	0.4	7.9
85–140	E	O_2^+, NO^+	2×10^5	0.4	7.9
140–200	F_1	NO^+, O_2^+, O^+	4×10^5	0.9	7.8
200–1200	F_2	O^+, N^+	2×10^6	1.4	7.5
1200–3400	Heliosphere	He^+	1×10^4	3.7	7.3–6.4
3400	Protonosphere	H^+	1×10^3	5.6	6.4

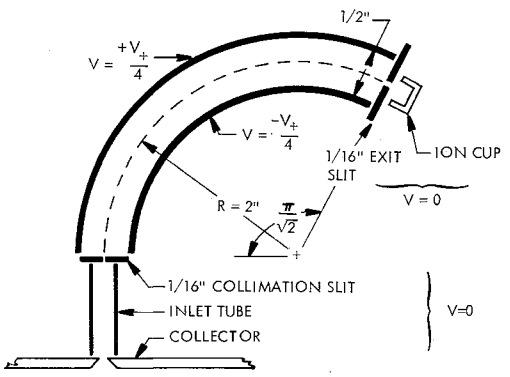

Fig. 2 Schematic of 127° analyzer.

to the difference between V_p and the ion source potential V_+. Also, the difference between V_p and the spacecraft potential V_s is a controlling factor in the electrical plasma-vehicle interaction.

Indicators of V_p include the potentials of immersed neutralizer (within the source), floating collector, floating emissive probes, and Langmuir probe data. Precise measurements of local values are obtained from the emission characteristic of the emissive probe.[1,6]

In general, outside the "injection region" of the neutralizer, along any radius, V_p is nearly constant in the central uniform-density region of the beam and decreases uniformly from there out to the chamber walls. Along the axis, it gradually decreases from the source to the floating collector.[7]

C. Electron Temperature in Plasma Beam

The kinetic energy distribution of neutralizing electrons is Maxwellian for well-neutralized beams, with a characteristic temperature T_e approximately equal to that of the electron emitter. In the absence of magnetic fields, T_e in downstream portions of the beam may drop well below this value. On the other hand, T_e may be increased by injecting the electrons through an abnormally large potential, as is done with neutralizers withdrawn from the beam.[9]

The collection characteristic of 1- to 5-mil tungsten wire probes provides a measure of T_e. These Langmuir probes[10] should have a constant work function, especially if T_e is low. Therefore, they are electrically heated to just below thermionic emission temperature. Experiments demonstrate that corrections for the directed motion of the plasma to standard Langmuir probe data analysis are not required to obtain the desired accuracy.

D. Ion Velocity

Measurements of v_+ are needed to demonstrate that the desired average velocity and velocity profile have been achieved for simulation. They also identify the major particle species in the beam.

1. *Ion time of flight*

The ion source potential has a 60-cps rectangular waveform. Current collected by a large downstream j_+ probe provides a time-of-flight measurement of q/M_+. From it, for example, continuous information of the relative abundances of N^+ and N_2^+ in a nitrogen plasma beam is available. Resolution of this mass measurement is complicated by the rise time of V_+, by dispersion in the plasma beam front, by displacement currents from the approaching plasma front (reduced when a j_+ grid is used), by uncertainty in V_p, and by noise signals.[8] Nevertheless, agreement within 5% is common between time-of-flight measurements and calculations from net acceleration potential corrected for rise time.

2. *Retarding potential analyzer*

The large Faraday-cup-type probe used for retarding potential measurements of ion energy is indicated in Fig. 1. It has a guard ring around the collector and a grid over the entrance aperture maintained sufficiently negative to reflect electrons. The collector and guard ring are swept through a range of positive voltages, and collected ion current is plotted against this potential. The derivative of this function is the net acceleration potential spectrum. Particles of different q/M_+ are not distinguished. This instrument is only used for low-density beams as it is less accurate and convenient than the following one.

3. *127° electrostatic analyzer*

Figure 2 is a diagram of a 127° electrostatic analyzer[11] used to measure ion velocity distributions. It also measures the net acceleration potential of a charged particle, and cannot distinguish between charge-to-mass ratios. Unlike the retarding-potential probe, its direct measurement is useful where the ion energy is a rapidly varying function of time. This is accomplished by observing the output with an oscilloscope for fixed analyzer deflection voltage. The small apertures necessary to produce 5% energy resolution result in small detected currents. Consequently, a driven-shield cathode follower at the ion cup reduces impedance and maximizes the frequency response of the output. Details of an experiment using the 127° analyzer to study time varying ion velocity distributions are discussed in Sec. V.C.

E. Ion Divergence Analyzer

This instrument measures the angular distribution of ions arriving at the test location. Normally they will be virtually paraxial, but, as will be discussed in Sec. V, it is sometimes desirable to introduce an angular spread in their flow. As shown in Fig. 3, the device consists of a rectangular aluminum box with an entrance aperture in one end and six collection rings at the other. In front of the rings is a wire screen of 2-mil tungsten with $\frac{1}{8}$-in. spacing.

In operation, the box itself is at or near V_p, the rings are held near ground potential by 100 $K\Omega$ resistors, and the screen basis is ~ -20 v. This repells plasma electrons and suppresses any secondaries from the rings. A multitrace oscilloscope across the 100 $K\Omega$ resistors allows a continuous measurement of the ring currents.

Three basic factors limit the analyzer performance. Each is sufficiently small to be neglected in the experiments of Sec. V.E., provided that the beam has a uniform j_+ in the region

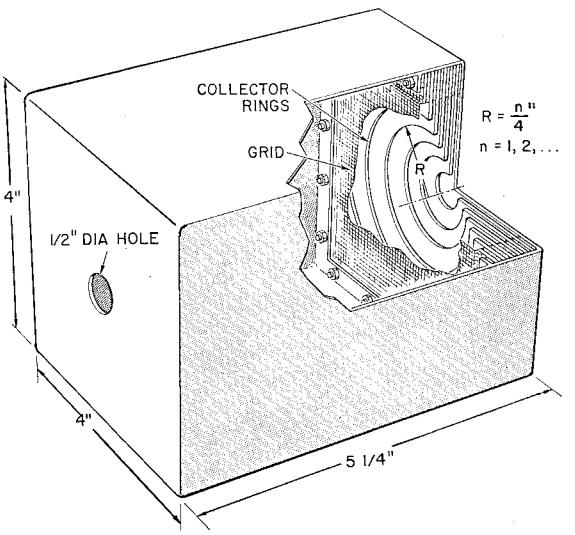

Fig. 3 Perspective of ion divergence analyzer.

of interest and a smooth angular distribution over a range of $\sim 8°$ or more from the axis. Uniform j_+ is always obtained near the beam center, and the sources of ion divergence discussed in Sec. V may be expected to produce a smooth distribution of angles. The following remarks note the effects of these factors when the range of angular divergence is less than $\sim 8°$.

The discrete width of the individual rings requires that an ion trajectory passing through the center of the aperture have an angle in excess of $2\frac{3}{4}°$ to be recorded as other than paraxial. When the total spread of ions entering at the aperture center is $< 8°$, only three rings measure current.

The diameter of the entrance aperture, if large enough to obtain measurable ring currents, allows off-axis ions to be collected on inappropriate rings. Under the assumptions of uniformity, it is possible to calculate this ring current distribution "broadening" from a particular source of diverging ions.

The "electrostatic lens" effects created by plasma sheaths in and around the aperture are perhaps the most involved. Experiments show that, as expected, biasing the box below V_p increases ion divergence, whereas biasing the box above V_p produces an inward focusing effect. Small changes in aperture potential produce observable shifts in ring currents. Therefore work function patchiness near the aperture could be detrimental, if present. In the data given in Sec. V.E., the box was biased ~ 1 to 2 v above V_p, and an inward focusing effect on the ion trajectories was evidenced by a small maximum in central ring current from a beam of small divergence. This compensated any small beam spreading forces due to electron pressure effects inside the analyzer. A second condition, employed in other experiments, allowed the box to assume its floating potential, which is $\sim 2kT_e/q$ negative with respect to the plasma if surface patch and wake effects[1] are disregarded. The additional noise signals encountered in this condition were reduced by capacitively coupling the box to ground. For over-all experimental convenience, the floating condition would be recommended.

In summary, these aspects of analyzer performance should be placed in perspective by noting that angular divergence in plasma wind-tunnel streams represents a second-order refinement. As such, construction of a more elaborate instrument would not, in general, be justified.

IV. Beams Produced and Their Properties

A. Ion Sources

Two types of ion source have been used in plasma wind-tunnel studies. In one, cesium ions are formed by contact ionization at the surface of a 2.5-cm-diam porous tungsten disk and accelerated by means of a planar wire mesh grid.[1,7-9] The other source is of the electron-bombardment type and is a flight model of the NASA Lewis Research Center, Kaufman ion rocket[6,12,13] modified by the addition of a gas inlet tube so that beams of various gas ions can be produced. Normal average divergence away from the beam axis of beams from these sources is $\sim 3°$ and $\sim 10°$, half-angle, respectively.

B. Properties of Beams Produced

In general, there are six parameters that specify a plasma beam for simulation purposes: 1) average ion velocity $\langle v_+ \rangle$; 2) ion density at test location n; 3) diameter of uniform ion density region at test location D_b; 4) ion mass constitutents M_+; 5) ion velocity profile $v_{+,\mathrm{th}}$, T_+, or ΔW; and 6) electron temperature T_e. Most of these parameters are interrelated, and sometimes a compromise between desired values of two or more of them must be made.[7] The contact and bombardment sources behave differently, so they will be discussed in turn.

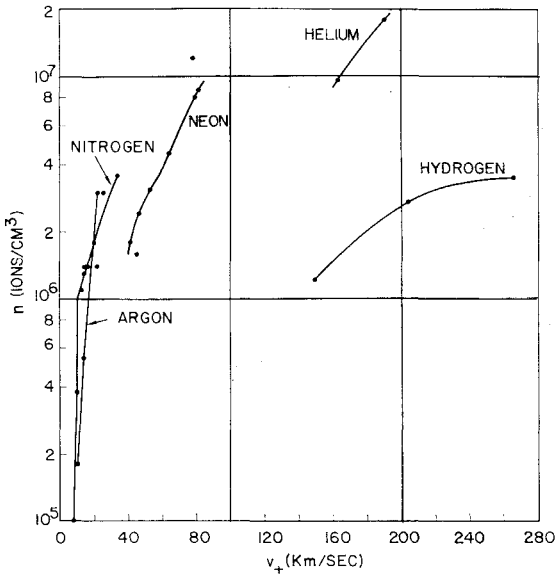

Fig. 4 Maximum uniform plasma density available over 30-cm-diam area at 1.6 m from the electron-bombardment source vs ion velocity for several gases.

1. *Contact ion source beams*

Because of the relatively large mass of Cs 133, velocities in the neighborhood of 8 km/sec are attained with convenient acceleration voltages (~ 41 v). The ion current magnitude is, of course, a function of this voltage, but it is even more strongly dependent on accelerator-grid to disk spacing and the quality and temperature of the disk itself. Without difficulty, D_b of 28 cm is obtained at 8 km/sec with $n \sim 10^7$ ions/cm^3, and this density may be increased if required.

When Cs is used for ionospheric simulation, the required densities are ~ 10 greater than ionospheric densities because of mass number scaling from 13 to 133. This is discussed along with other scaling relationships among vehicle size, ion velocity, ion density, ion mass, and vehicle potential in Ref. 1.

The cesium beam contains only Cs^+ and has virtually a line spectrum of velocity. Increasing T_e increases D_b, and it is usually set between 0.25 ev and several ev.[7]

2. *Electron-bombardment ion source beams*

The electron-bombardment ion source does not have provision for varying the accelerator spacing, and, therefore, the ion current produced is a function only of discharge conditions and acceleration voltages. Discharge conditions depend on the gas in use, discharge voltage, magnetic field, and cathode temperature. Figure 4 shows maximum densities obtained with various gases as a function of ion velocity. If less than the maximum density is required at a particular velocity, the discharge intensity is reduced. A typical value of D_b is 30 cm, and a 30% reduction in n occurs at ~ 58 cm diam.

In addition to the A, N_2, Ne, He, and H_2, which appear in Fig. 4, beams of O_2 and mixtures of CO_2 and A have been produced. Cathode lifetime is about 1 hr when O_2 is used (as compared to tens of hours with other gases), so that experiments with O_2^+ beams are limited in duration.

Table 2 lists beam constituents, beam energy (qV_0), and width of ion energy distribution $\Delta W'$ for various gases. This width is the difference between energies for which the analyzer output is 0.1 of its peak value.

The values of V_0 shown produced sufficiently dense beams to allow convenient use of the 127° analyzer and do not represent specific simulation conditions. Smaller values of $\Delta W'$ occur as V_0 is decreased.

Production of 10 km/sec beams from H_2 and He requires acceleration potentials of ~ 1 v. The energy spread from the

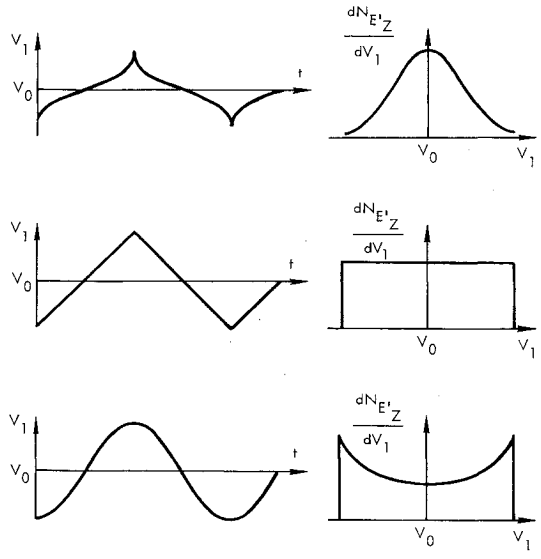

Fig. 5 "Longitudinal" energy distributions produced by various perturbation potential waveforms.

discharge is several times this value, so that the present source is not suitable for these beams. In all of these beams, an immersed neutralizer was used, so that $T_e \leq 0.25$ ev.

V. Simulation of Ion Temperature

The relative motion between a vehicle moving through the ionosphere and a particular ion or electron is the resultant of both the vehicle velocity and the thermal velocity of the particle. As discussed in Sec. II, below the heliosphere the relationship

$$v_{e,\text{th}} \gg v_s \gg v_{+,\text{th}} \tag{1}$$

is obtained. Therefore the relative velocities between the vehicle and the ions in the plasma are essentially v_s with a small randomizing ion thermal component, whereas the relative velocities between the vehicle and the electrons are almost totally randomized in direction and have magnitudes of $\sim v_{e,\text{th}}$. It follows that simulation of this small randomized ion velocity represents a refinement that may be omitted in many experiments. However, it is interesting first to calculate $v_{+,\text{th}}$ as seen from a vehicle and then examine experimental techniques for its simulation.

A. Thermal Velocities from a Moving Frame of Reference

For an assumed Maxwellian distribution of the ions in the laboratory frame, the velocity distribution of the ions is given by

$$d^3N_{v_x v_y v_z} = N\left(\frac{M_+}{2\pi kT_+}\right)^{3/2} \times \exp\left[-\frac{M_+}{2kT_+}(v_x^2 + v_y^2 + v_z^2)\right] dv_x dv_y dv_z \tag{2}$$

where M_+ is the ion mass, N is the total number of ions in the system, and T_+ is the ion temperature. If v_s is assumed to be in the negative z direction, and if the primed coordinates denote the vehicle reference frame, then the ion velocity distribution, as seen by an observer moving with the vehicle, is

$$d^3N_{v_x' v_y' v_z'} = N\left(\frac{M_+}{2\pi kT_+}\right)^{3/2} \times \exp\left\{-\frac{M_+}{2kT_+}[v_x'^2 + v_y'^2 + (v_z' + v_s)^2]\right\} dv_x' dv_y' dv_z' \tag{3}$$

where $v_z' = v_z - v_s$. Note that the sign of v_s is defined in the laboratory frame.

The first considerations will relate to temperature simulation in the "longitudinal" or z direction with the x and y components of the velocity neglected. That distribution is given by

$$dN_{v_z'} = N\left(\frac{M_+}{2\pi kT_+}\right)^{1/2} \exp\left[-\frac{M_+}{2kT_+}(v_z' + v_s)^2\right] dv_z' \tag{4}$$

Denoting $E_0 = M_+ v_s^2/2$ and $E_z' = M_+ v_z'^2/2$, the distribution becomes

$$dN_{E_z'} = N\left(\frac{M_+}{2\pi kT_+}\right)^{1/2} \exp\left\{-\frac{1}{kT_+}[(E_z')^{1/2} - (E_0)^{1/2}]^2\right\} \times \frac{dE_z'}{(2M_+E_z')^{1/2}} \tag{5}$$

when the appropriate square roots of E_0 and E_z' are chosen. The energy "width" of this distribution is roughly described by the points at which $[(E_z')^{1/2} - (E_0)^{1/2}]^2 = kT_+$, since $(2M_+E_z')^{-1/2}$ is only slowly varying through this interval:

$$\Delta W' \simeq 4(E_0 kT_+)^{1/2} \tag{6}$$

As before, kT_+ is the thermal energy of the ions in the laboratory frame. It is seen that the energy spread of oncoming ions apparent from a vehicle moving with v_s is generally larger than $\Delta W \simeq 2\ kT_+$, the energy spread in the fixed frame. Thus, the simulation of "longitudinal" ion temperature requires larger velocity perturbations than Eq. (1) suggests. For example, to simulate the motion of a vehicle at 10 km/sec through a N_2^+ plasma at 1500°K ($2kT_+ = 0.26$ ev), the N_2^+ stream in the plasma wind tunnel should have a total width in the acceleration potential of ~ 5.5 v centered about a mean acceleration potential of 14.5 v.

B. Theory of Longitudinal Thermal Velocity Simulation

The simulation of T_+ in a plasma wind tunnel requires, in the longitudinal direction, an energy distribution whose width is given by Eq. (6). In the case of the electron-bombardment source, a significant part of this $\Delta W'$ may arise from the fact that ions are formed in a region in which potential gradients exist. Furthermore, these gradients are, to some extent, influenced by the magnitude of the discharge potential and magnetic field, thereby allowing some control of the energy spread. Typical values of $\Delta W'$ are listed in Table 2.

The natural energy spread of ions from the contact ionization source is, on the other hand, negligible. It arises primarily from the emitter surface tempeature. When a constant amount of kinetic energy is added to each ion formed, the accelerated group has the same energy spread as before, $\Delta W = \Delta W'$. Equation (6), therefore, will indicate the approximate temperature of ions in the stationary frame, which is simulated by their thermal spread at the contact source, namely

$$T_+ = (\Delta W')^2/(16kE_0) \tag{7}$$

As a typical example, consider an $\langle v_+ \rangle$ of 10 km/sec ($E_0 = 69$ ev for Cs) and an emitter surface temperature of

Table 2 Beam constituents and ion energy spread of various input gases

Gas	Ions	$\Delta W'$, ev	V_0, v
Hydrogen	12% H^+, 88% H_2^+	...	...
Helium	5% He^{++}, 95% He^+	...	...
Nitrogen	28% N^+, 72% N_2^+	10	68
Oxygen	~14% O^+, ~86% O_2^+ (tentative)	...	...
Neon	3% Ne^{++}, 97% Ne^+	14	181
Argon	4% A^{++}, 96% A^+	8	86

1500°K ($\Delta W' = 0.15$ ev). The simulated longitudinal temperature in the accelerated flow is then ~ 0.1°K.

To increase the simulated longitudinal ion temperature of either source type, a periodic perturbation potential V_1 may be superimposed on the accelerating potential V_0 that is otherwise constant during its periods of positive value: $V_+ = V_0 + V_1$. Then ions exhausted at various times undergo differing amounts of acceleration. The following discussion will first treat the choice of frequency and then the choice of waveform for V_1.

The question of frequency is to assure that the velocity distribution of ions arriving at the object under test is time invariant. Analysis is simplified by assuming a sinusoidal waveform: $V_1 = \tilde{V} \sin\omega t$. If $V_p = 0$, and $\tilde{V} \ll V_0$, then the velocity of ions emerging at time t is

$$v_+ \simeq v_s[1 + (\tilde{V}/2V_0) \sin\omega t] \tag{8}$$

where

$$v_s = (2qV_0/M_+)^{1/2}$$

As the ions move downstream, the velocity modulation introduced at the source will create "bunching" in the stream. Indeed, the present configuration may be termed an "ion klystron," and the conventional large signal klystron analysis may be applied.[14] The point downstream at which bunching first occurs is

$$\Lambda \simeq (v_s/\omega)(2V_0/\tilde{V}) \tag{9}$$

The desired condition is that the plasma stream possess no such bunching but rather a density invariant in time. Bunching at points farther downstream is increasingly diffuse; adequate mixing may be achieved if the distance l separating the plasma source from the vehicle is much greater than Λ. Experimental verification is presented in Sec. V.C.

The frequency requirements have been developed using a sinusoidal V_1. As indicated later, this waveform, although producing a spread in the ion energies, does not produce the accelerated Maxwellian required for an ideal longitudinal temperature simulation. The required wave orm is obtained from rewriting Eq. (5) using $V_+ = E_z'/q$ and $V_0 = E_0/q$. Again considering $V_1 \ll V_0$, one obtains

$$dN_{E_z'} \simeq N\left(\frac{q}{4\pi kT_+}\right)^{1/2} \exp\left[-\frac{q}{kT_+}\frac{V_1^2}{4V_0}\right]\frac{dV_1}{V_0^{1/2}} \tag{10}$$

In this case, or if the source is running emission limited, $q\,dN/dt = i_+$ is constant. Using this relation and the chain rule for derivatives yields an easily integrated differential equation. Its solution is

$$t = \frac{qN}{2i_+}\,\mathrm{erf}\left[\left(\frac{q}{4\pi V_0 kT_+}\right)^{1/2} V_1\right] \tag{11}$$

Thus the required waveform is the inverse of the error function. Of course, the choice of $t = 0$ is arbitrary. The inequality $V_1 \ll V_0$ begins to fail near time values of plus and minus unity, and from the problem it is known that V_1 reaches some maximum absolute value. As a matter of electronic convenience, successive waveforms would probably be reflected about the vertical axis of symmetry to produce a continuous periodic wave train. As discussed previously, its maximum period is determined by the requirement that $l \gg \Lambda$. Figure 5 shows this waveform and the velocity distributions produced by two other more convenient waveforms. In the case of these non-Maxwellians, "temperature" may be defined by equating $\langle (v_+ - v_{+,0})^2 \rangle$ of the distribution to $\langle v_z^2 \rangle$ of a Maxwellian.

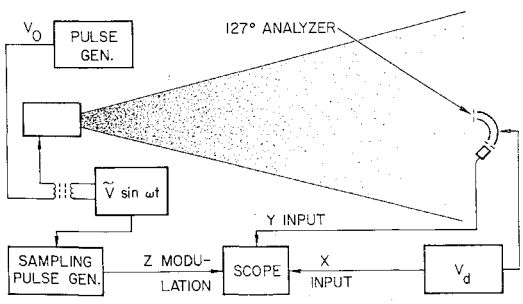

Fig. 6 Schematic diagram of longitudinal thermal velocity simulation experiment.

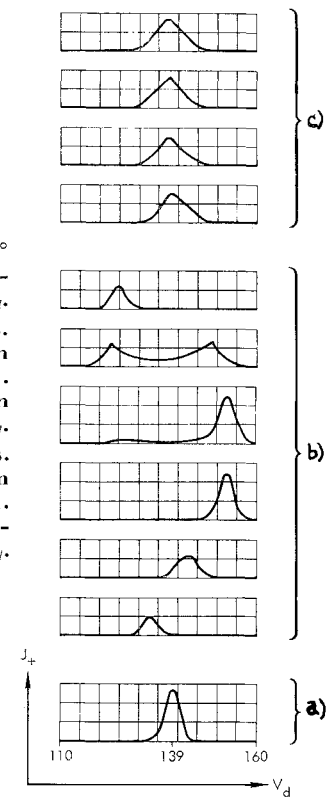

Fig. 7 a) Output of 127° analyzer. Perturbation voltage $V_1 = 0$; $V_+ = 2\,V_d$. b) $\tilde{V}$ is 32 v, $f = 25$ kcps. Shots at several times t in the range $nT \leq t \leq nT + 1$. Poor temperature simulation is obtained; $V_+ = 2\,V_d$. c) $\tilde{V}$ is 9 v, $f = 250$ kcps. Shots at several times t in the range $nT \leq t \leq nT + 1$. Good temperature simulation is obtained; $V_+ = 2\,V_d$.

C. Longitudinal Thermal Velocity Simulation Experiment

To demonstrate that time-invariant temperature simulation could be achieved through the rapid variation of the source potential, the experimental configuration in Fig. 6 was assembled. The perturbation potential V_1 was $\tilde{V} \sin\omega t$, and V_0, $\tilde{V}$, and ω could be varied. The output of the 127° analyzer was used as the vertical input to an oscilloscope; the horizontal sweep was derived from the analyzer deflection voltage V_d. The deflection voltage was swept manually. The scope beam was blanked so that the trace was only visible during a 1-μsec sampling pulse that was delayed from the zero crossing of V_1. Each of the scope face photographs (Fig. 7) represents the locus of samples of the output signal for a single sweep of V_d through the range of interest with a fixed value of time delay. Therefore, they are plots of the ion energy spectrum at different phases of V_1. The horizontal scale begins at 110 v and each division represents 5 v. The physical parameters of the analyzer are such that $V_+ = 2\,V_d$.

Figure 7a was taken with $V_1 = 0$, and the peak occurred at $V_d = 139$. Such values of V_d, corresponding to $\langle V_+ \rangle$ of an unperturbed beam, agree within 3% with time-of-flight measurements that have been carefully corrected for the error sources mentioned in Sec. III.D.1. However, the shape of the energy spectrum in Fig. 7a is more representative of the analyzer "window" than of the energy spectrum of the unperturbed Cs^+ beam. Specifically, calculations show that, in the absence of space-charge expansion of the beam while traversing the spectrometer, a monoenergetic beam will ex-

hibit a line width of 3% in energy at half maximum and that space charge increases the width to 5% with 10^7 ions/cm^3 at 300 ev. (At 10^6 ions/cm^3 or less this latter effect is unimportant at this velocity.) Nevertheless, the analyzer is very useful in observing the effect of a perturbation voltage, as comparison of Figs. 7b and 7c to Fig. 7a will show.

In Fig. 7b, a 25-kc, 32-v peak signal has been added to V_0. Here V_1 varies the beam energy 23%, so that the spectrometer easily distinguishes its effect. The distance l is 191 cm. Starting at the top of the group, each photograph was taken with a longer delay time from the zero crossing of V_1; the bottom trace was taken almost one period of V_1 later. At first only ions that have been slowed down are present (compare to Fig. 7a). Then a mixture of energies appears, followed by a single group of "fast" ions (the maximum attained). As time progresses, this group becomes less and less energetic until the minimum energy that began the sequence is attained.

To relate these spectra in detail to the phase of the V_1 is complicated. But this is not necessary to see that these values of ω, $\tilde{V}$, and V_0 did not lead to a time-invariant mixture of energies which could be regarded as a simulated ion temperature. Nor should they be expected to, since l/Λ is 0.87 in this case. Notice that, if all six traces are added, the shape of the resulting energy distribution is similar to that of Fig. 5c.

When the frequency was increased to 250 kc, even though V_1 was reduced to 9 v peak, $l/\Lambda = 2.4$. Again photographs were taken at different times throughout a period of V_1, and representatives are shown in Fig. 7c. Now the peak energy occurs at ~139 v (just as with $V_1 = 0$ in Fig. 7a) regardless of the phase of V_1. The effect of V_1 has been to broaden the energy distribution and simulate an ion temperature. However, in this case, V_1 (the maximum available at this frequency) is only 3.6% of V_0, and the resolution of the analyzer is important.

D. Theory of Transverse Thermal Velocity Simulation

As indicated in Eq. (3), the radial ion velocity $v_r = (v_x^2 + v_y^2)^{1/2}$ is unaffected by the relative motion between the plasma and the spacecraft. Therefore a perfect simulation of the ion temperature in the transverse direction would produce

$$dN_{v_r} = N \frac{M_+}{kT_+} v_r \exp\left(-\frac{M_+ v_r^2}{2kT_+}\right) dv_r \qquad (12)$$

As in the longitudinal case, something short of the ideal may be satisfactory for an experiment and more easily produced.

In fact, the use of an ion source of finite extent provides some transverse velocity. In both source types that have been described, each element of accelerator grid acts as a separate plasma source. Because of the electrostatic lens action of this grid and the effects of energetic neutralizing electrons, the angular velocity distribution from each subbeam is essentially uniform up to an angle θ.

However, the maximum v_r of a particle arriving at an on-axis point downstream cannot be greater than $\sim v_+ r_{is}/l$. Therefore

$$v_{r,\max} = v_+ r_{is}/l \quad \text{or} \quad v_+ \sin\theta \qquad (13)$$

whichever is the smaller.

The $\langle v_r \rangle$ of this uniform angular distribution from the source is $\frac{2}{3} v_{r,\max}$. To define an effective temperature for the residual transverse velocity spectrum of a source-object configuration, this average value of radial velocity is equated to that of Eq. (12):

$$T_{\text{eff}} = 8 M_+ v_{r,\max}^2 (9\pi k)^{-1} \qquad (14)$$

where $v_{r,\max}$ is given by Eq. (13).

Whether this temperature is sufficient in a given experiment depends on the values θ, l, r_{is}, and v_+. The choice of r_{is} and l in turn depends on the size of the object under test. The value of θ depends on the magnitudes of acceleration voltages, grid spacing, grid hole size, and T_e. In general, it is ~2° for the contact ionization source and ~8° for the electron-bombardment source.

The values of the other parameters, which are selected to simulate the principal features of ionospheric travel, lead to a simulated transverse temperature of a few hundred degrees Kelvin or less. Since a value in the range 1000°–2000°K (relative to $v_+ \simeq 8$ km/sec) is usually desired, some artificial technique to increase the range of v_r must be employed.

The technique investigated consisted of placing a large, coarse grid in the beam between the source and object. With a suitable negative potential on the grid, the ion flow interacted with these electric field centers, increasing their transverse momentum distribution. The design of such a grid mesh size, mesh shape and thickness, downstream location, and potential is somewhat involved since space-charge calculations are required. After preliminary calculations, the configuration described in the next section was used to demonstrate the technique.

E. Transverse Thermal Velocity Simulation Experiment

The natural transverse thermal velocity distribution of 180-v N_2^+ plasma from the 11-cm electron-bombardment source was measured with the ion divergence analyzer. Its distance from the source was 1.6 m. The ratio of currents, ring 2/ring 1, was 0.62. Because this configuration represented an angular distribution of less than 6°, the analyzer entrance aperture size could not be neglected. Using the previously discussed uniformity assumptions, an expression was derived for the ring currents due to an off-axis source point, using the actual areas of collector rings and aperture. This expression integrated over the entire source area predicted 0.5 for this ratio. Agreement within 20% for the measurement of low-divergence beams is satisfactory.

This source to object configuration corresponded to a residual transverse temperature of 1450°K at the value of v_+ used (35 km/sec). However, transverse temperature scales as v_+^2, so that at 8 km/sec the temperature would have been 74°K. The experiment was done with the high value of v_+ to provide a more convenient signal level from the analyzer ($n \simeq 2 \times 10^6$ ions/cm^3 at the analyzer location).

To enhance this transverse velocity distribution, a 1-m square cross grid of 10-mil wire spaced 2.5 cm was placed in the vacuum tank 53 cm upstream of the analyzer. This location was convenient and met the following two conditions: If the scattering grid is too close to the analyzer ($< \sim 10$ wire spacings), the beam at the entrance aperture may not be homogeneous; if the grid is too far, the maximum transverse velocity of particles entering the analyzer becomes small as in the case of the distant ion source.

Figure 8 shows the ratios of currents to rings 2, 3, and 4 to the ring 1 current, with scattering grid potential as the parameter. The currents to rings 3 and 4 for the −20-v case include a large percentage of noise.

To interpret these data in terms of a Maxwellian distribution, calculations of ring currents were made which assumed transverse Maxwellians of various temperatures at the entrance aperture (now assumed infinitely small in area). Under this assumption,

$$v_r = v_+ r/L \qquad (15)$$

where L is the axial length of the divergence analyzer, and r is the radial location of the point at which the ion is collected. Substituting this expression into Eq. (12) and integrating between values of r that represent the dimensions of each collector ring yields the current ratios also shown in Fig. 8. Apparently −80 v on the grid approximates 20,000°K rather well at $v_+ = 35$ km/sec. Were this same distribution of ring currents observed with a v_+ of 8 km/sec, it would correspond to ~1000°K. Thus, the scattering grid is capable of an

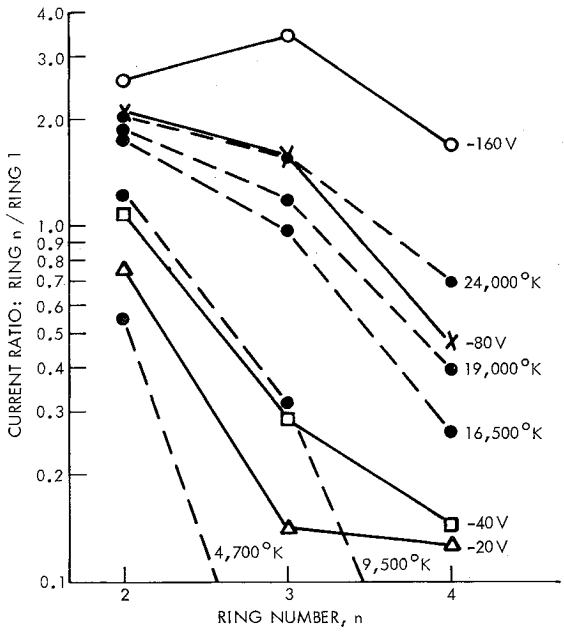

Fig. 8 Solid lines represent measured ratios of ring 2, 3, and 4 currents to ring 1 current for various scattering grid potentials. Broken lines represent calculated values of these ratios for various transverse temperatures.

effective simulation of the transverse thermal velocity distribution that an orbiting spacecraft would encounter in the ionosphere.

VI. Summary and Conclusions

Spacecraft travel through the region of the ionosphere below the heliosphere may be simulated in vacuum chambers by directing a moving plasma stream against a stationary vehicle. For this purpose streaming plasmas of H_2, He, N_2, O_2, Ne, A, CO_2, and mixtures thereof have been synthesized with an electron-bombardment ion source. A contact ion source produced monoenergetic cesium beams, useful when line velocity spectra were required. Pertinent properties of the ionosphere have been reviewed and diagnostic instruments for determining these same properties in the synthesized streams described.

The extent to which ion thermal velocity in the ionosphere effects the relative motion between the ions and a vehicle has been calculated. It was shown that in order to simulate an ion thermal velocity distribution along the direction of spacecraft motion a considerable beam energy width is required. A sinusoidal fluctuation in the beam acceleration potential with magnitude and frequency which met derived criteria successfully simulated a longitudinal temperature. A scattering grid placed between the plasma source and test object provided for simulation of a transverse temperature. The controlled operation of these plasma sources over a wide range of parameters permits laboratory study of the interaction of material bodies moving through dilute plasmas and the calibration of onboard instrumentation for the diagnosis of the dilute plasmas of space.

References

[1] Hall, D. F., Kemp, R. F., and Sellen, J. M., Jr., "Plasma-vehicle interaction in a plasma stream," AIAA J. **2**, 1032–1039 (1964).

[2] Hanson, W. B., "Structure of the ionosphere," *Satellite Environment Handbook*, edited by F. S. Johnson (Stanford University Press, Stanford, Calif., 1961), pp. 27–46.

[3] van de Hulst, H. C., de Jager, C., and Moore, A. F., (eds.) *Space Research II* (North-Holland Publishing Co., Amsterdam, 1961), Pt. VIII, pp. 889–1017.

[4] Hanson, W. B., "Upper-atmosphere He ions," J. Geophys. Res. **67**, 183–188 (1962).

[5] Bourdeau, R. E., Whipple, E. C., Jr., Donley, J. L., and Bauer, S. J., "Experimental evidence for the presence of He^+ based on Explorer VIII satellite data," J. Geophys. Res. **67**, 467–475 (1962).

[6] Kemp, R. F., Sellen, J. M., Jr., and Pawlik, E. V., "Neutralizer tests on a flight-model electron-bombardment ion thrustor," NASA TN D-1733 (July 1963).

[7] Sellen, J. M., Jr., Bernstein, W., and Kemp, R. F., "The generation and diagnosis of synthesized plasma streams," Rev. Sci. Instr. **36**, 316–322 (1965).

[8] Sellen, J. M., Jr. and Kemp, R. F., "Cesium ion beam neutralization in vehicular simulation," ARS Preprint 61-84-1778 (June 1961).

[9] Bernstein, W. and Sellen, J. M., Jr., "Oscillations in synthetic plasma streams," Phys. Fluids **6**, 1032–1033 (1963).

[10] Langmuir, I. and Mott-Smith, H. M., "The theory of collectors in gas discharges," Phys. Rev. **28**, 727–763 (1926).

[11] Bainbridge, K. T., *Experimental Nuclear Physics*, edited by E. Segre (John Wiley and Sons, New York, 1953), Vol. 1, pp. 566–575, Case $y = 1$.

[12] Kaufman, H. R., "An ion rocket with an electron-bombardment ion source," NASA TW D-585 (January 1961).

[13] Reader, P. D., "Experimental effects of scaling on the performance of ion rockets employing electron-bombardment ion sources," ARS J. **32**, 711–714 (1962).

[14] Field, L. M., "Generation of high-frequency energy," *Foundations of Future Electronics*, edited by D. B. Langmuir and W. D. Hershberger (McGraw-Hill Book Co., Inc., New York, 1961).